



Effect of Coolant Inlet Mode on Heat Transfer Characteristics of a Twin-web Turbine Disc Cavity

Y. T. Guo, S. F. Wang[†] and W. J. Shen

College of Energy and Power Engineering, Nanjing University of Aeronautics and Astronautics, Nanjing, 210016, China

[†]Corresponding Author Email: sfwang@nuaa.edu.cn

ABSTRACT

Twin-web turbine discs have been the subject of recent research in an effort to lighten the weight of and boost the efficiency of aero engines. This has motivated researchers to investigate other configurations for an expanded blade air supply and twin-web turbine discs. However, the new configuration's cooling mechanism is unclear. In this paper, the flow and heat transfer characteristics of two twin-web turbine disc systems, featuring distinct coolant inlet modes, are investigated through theoretical analysis and numerical simulation. The research results show that the central inlet mode leads to an uneven coolant distribution, a high convective heat transfer coefficient, and a high Nusselt number in the rotor–stator cavity. Meanwhile, the pre-swirl inlet mode improves cooling in the high-temperature region by disturbing the vorticity. Augmenting the dimensionless mass flow rate enhances the cooling efficiency via the notable jet effect, but it also escalates energy loss. As the rotational Reynolds number rises, the entrainment effect of the rotor assumes a dominant role, thereby reducing the swirl ratio. The increased turbulence parameter shifts the primary heat transfer driver from the rotor register to the jet effect, resulting in more uniform temperature changes and a reduced radial inhomogeneity. The pre-swirl inlet mode demonstrates an outstanding cooling performance overall.

Article History

Received June 28, 2024

Revised September 15, 2024

Accepted October 20, 2024

Available online February 4, 2025

Keywords:

Flow characteristic

Pre-swirl system

Turbulence parameter

Twin-web turbine disc cavity

Temperature uniformity

1. INTRODUCTION

Raising the gas temperature at the turbine inlet is a crucial step in the development of aero engines, as it increases the engine's thermal efficiency. Nevertheless, this method might drastically shorten the high-temperature component's service life (Kim & Song, 2019). Thus, there is an immediate need for better cooling techniques. Among these, the pre-swirl system provides premium coolant for cooling the turbine disc chamber and turbine blades (Gong et al., 2022).

Currently, the single-web turbine disc (SWD) cavity system is the primary focus of pre-swirl system research. Through theoretical analysis and experimental research on the energy conversion traits and heat transfer mechanism of multi-inlet and multi-outlet sealed-air pre-swirl systems, the alterations in power consumption and temperature drop in relation to the mass flow ratio and velocity of the system can be ascertained, providing a novel approach for evaluating and enhancing the design of low-power, low-temperature pre-swirl systems (Lin et al., 2021; Liu et al., 2021a; Lin et al., 2022; Ma et al., 2024). Research is mostly focused on the geometric parameters

of the pre-swirl nozzles, which include the nozzles' length, pre-swirl angle, and position radius (Lewis et al., 2008). Cascade blade nozzles, blade-hole nozzles, and two varieties of receiver holes with a blade form were created (Liu et al., 2021b; Liu et al. 2023, Kong et al., 2022). Furthermore, it has been discovered that the optimal radial position of the nozzles to minimize wind resistance and mixing loss is within the range of 0.80–0.96, depending on the pre-swirl nozzle height and supply hole height. Liao et al. (2014) developed an optimization model that maximized the pre-swirl efficiency while minimizing the overall pressure loss. A system that has its nozzles positioned relatively low on the radial plane reduces leakage flow, which raises the output power of the turbine (Zhou & Zhou, 2020). Zhang et al. (2016a) discovered that the system performs best and has the maximum adiabatic efficiency and total pressure loss when the pre-swirl angle is 20°. A unique twin-row nozzle design was developed by Xia et al. (2020). The high-speed swirl flow from the nozzles is received by the receiver holes, which then send it to the co-rotating cavity with blade supply porosity. When the pre-swirl nozzles and receiver holes are positioned in the same radial direction, the least amount of pressure loss is possible (Jarzombek et al., 2006).

NOMENCLATURE	
ACRONYMS AND ABBREVIATIONS	
H_0	height of disc hub
H_1	height of disc rim
R_0	inner radius of disc
R_1	outer radius of disc
R_2	center radius of receiver hole
R_3	radius of inlet arc (inside)
R_4	radius of inlet arc (outside)
S_0	width of inlet-mid
S_1	width of disc bottom
S_2	width of single disc edge
ΔT	excess temperature on the windward side
T_l	local temperature
T_{in}	temperature of inlet
u	local radial velocity
U	average radial velocity at the entrance
z	local axial position
D	one-third thickness of the Ekman layer
a	radial height of the entrance of the co-rotating cavity
s	axial width of the co-rotating cavity
Q	inlet flow rate in the co-rotating cavity
T_{max}	maximum temperature of the turbine disc
Sr	swirl ratio
V	speed of the coolant in the rotating cavity
ω	rotation speed of the rotating disc
Re_φ	rotational Reynolds number
ρ	density of the coolant
b	outer radius of the turbine disc
m	mass flow of the coolant
μ	dynamic viscosity of the coolant
C_m	dimensionless mass flow
T_{vr}	radial temperature non-uniformity coefficient
\bar{t}	average temperature of all feature points
S	temperature change
n	total number of feature points
t_i	temperature of the feature point
θ	normalized temperature
t_{max}	maximum value of the temperature range
t_{min}	minimum value in the temperature range
Nu	Nusselt number
q	heat flux
r	local radius
λ	thermal conductivity of the coolant
T_r	reference temperature
β	field synergy angle
\vec{v}	velocity field
$grad\vec{T}$	temperature gradient field
T^*	absolute total temperature of the coolant
T_{rel}^*	relative total temperature of the coolant
c_p	specific heat of coolant at constant pressure
h	convective heat transfer coefficient
λ_T	turbulence parameter
$Case_1^C$	change in case ₁ with dimensionless mass flow
$Case_1^R$	change in case ₁ with rotational Reynolds number
$Case_2^C$	change in case ₂ with dimensionless mass flow
$Case_2^R$	change in case ₂ with rotational Reynolds number
A	feature points on the outer wall of the front web
B	feature points on the inner wall of the front web
C	feature points on the inner wall of the front web
D	feature points on the outer wall of the back web
SUBSCRIPT	
φ	φ
z	z
r	r
rh	rh
ic	coolant in the inner cavity
mix	mixed coolant
1	variables related to case ₁
2	variables related to case ₂

At the location where the tangential velocity difference is the least, the receiver holes' peak flow coefficient value appears (Bricaud et al., 2007). In order to create a more uniform stress distribution, Yan et al. (2020) modified the receiver hole structure using the improved support vector regression surrogate model. Numerous studies on the pre-swirl system have successfully enhanced the single-web turbine disc's cooling capabilities; however, because of its thicker hub, the engine's internal cooling response remains sluggish, restricting our ability to further increase the aero engine's efficiency.

There is now renewed promise for increasing aero engine efficiency thanks to twin-web turbine discs

(TWDs) (Zhang et al., 2020). Though theoretical analysis and optimization techniques can be used, in-depth research on the structural characteristics of the disc cavity of a SWD cannot be directly applied to the disc cavity of a TWD (Zhang et al., 2017). In order to improve heat transfer, Zhang et al. (2016 b) created a model with curved ribs in the inner hollow. Their findings demonstrated a considerable decrease in the turbine disc's average temperature. A new kind of twin-web turbine disc with staggered needle fins placed close to the inner cavity and outflow has been proposed (Li et al., 2019, 2020). Multidisciplinary design optimization was performed, with the aim of minimizing weight and temperature while adhering to stress restrictions. Zhang

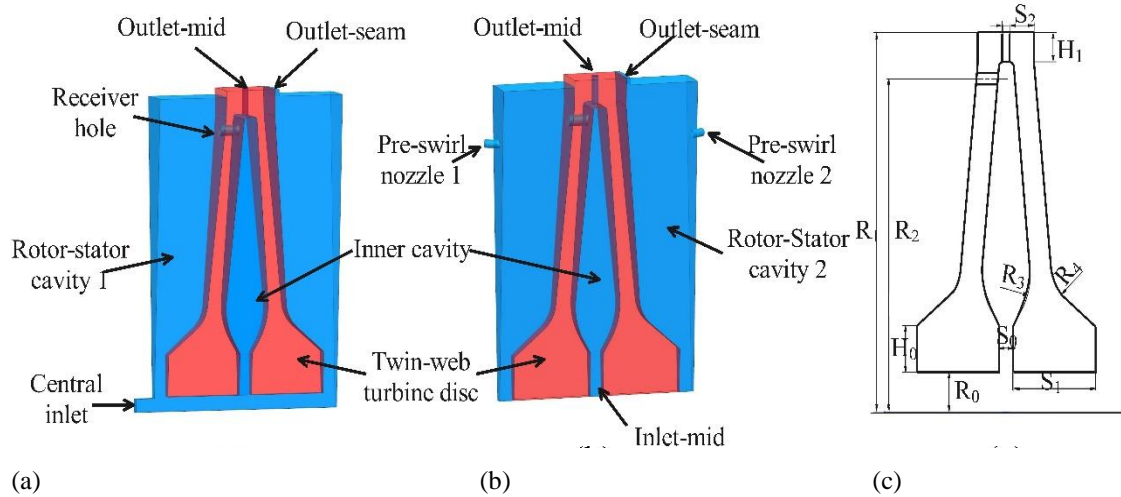


Fig. 1 Three-dimensional geometry of (a) Case₁, (b) Case₂, and (c) structural parameters of the TWD

Table 1 Geometric parameters of the TWD cavity system

Geometric parameter	Symbol	Unit	Design value
Height of disc hub	H_0	mm	31
Height of disc rim	H_1	mm	20
Inner radius of disc	R_0	mm	53.5
Outer radius of disc	R_1	mm	281
Center radius of receiver hole	R_2	mm	250
Radius of inlet arc (inside)	R_3	mm	50
Radius of inlet arc (outside)	R_4	mm	25
Width of inlet-mid	S_0	mm	10
Width of disc bottom	S_1	mm	58.8
Width of single disc edge	S_2	mm	20

and Li also employed a central inlet approach in their study. Furthermore, Ma et al. (2021, 2022) employed a large-radius pre-swirl system in a TWD turbine disc cavity system and investigated the impact of inlet flow ratio on cooling efficiency. As previously mentioned, prior research on TWD has primarily concentrated on improving heat transfer between the coolant and wall, has analyzed structure and operation parameters, and has only considered the coolant inlet condition as a fixed parameter. This previous research has neglected to take into account the impact of various coolant inlet modes on flow and heat transfer effects, which are the subject of this paper.

A systematic analysis of the heat transmission characteristics of the inter-rotor–stator system of the TWD cavity is presented in this paper, focusing on the effects of two inlet modes—central inlet and large-radius inlet pre-swirl. Under the same turbulence settings, the sensitivity of dimensionless mass flow and rotational Reynolds number and their effects on heat transfer characteristics are investigated. Additionally, a parameter feature importance analysis is carried out, to determine how the heat transfer properties are affected by the radial height and tangential angle of the pre-swirl nozzles and receiver holes.

2. MODEL AND METHOD

2.1 Calculation Model

This research established a TWD model with receiver holes based on reference (Ma et al., 2021). There are two domains in the TWD numerical convective heat transfer model: a fluid domain and a solid domain. All fluid domains are subjected to the same boundary conditions, in order to qualitatively investigate the impact of intake convection heat transfer characteristics. Accordingly, the coolant enters the inner cavity, fluid domain 1, and fluid domain 2.

The fluid domain is only slightly modified, while the turbine disc's stress distribution remains essentially intact. Various coolant inlet modes are used to discuss the potential for cooling. The coolant in rotor–stator cavity 2 exits through the outlet seam on the disc-edge side, whereas the coolant in cavity 1 exits through the mixing of the receiver hole and the inner cavity through the outlet-mid. In this paper, Case₁ and Case₂ represent the central inlet and high radius inlet pre-swirl modes, respectively. Schematic diagrams and structural parameters are shown in Fig. 1 and Table 1. The 1/60 TWD model is used in this paper to conserve computing resources. Dynamic cavity 1 and the inner cavity are integrated into one, named fluid domain 1. The rotor–stator cavity 2 is fluid domain 2. The TWD is considered to be the solid domain.

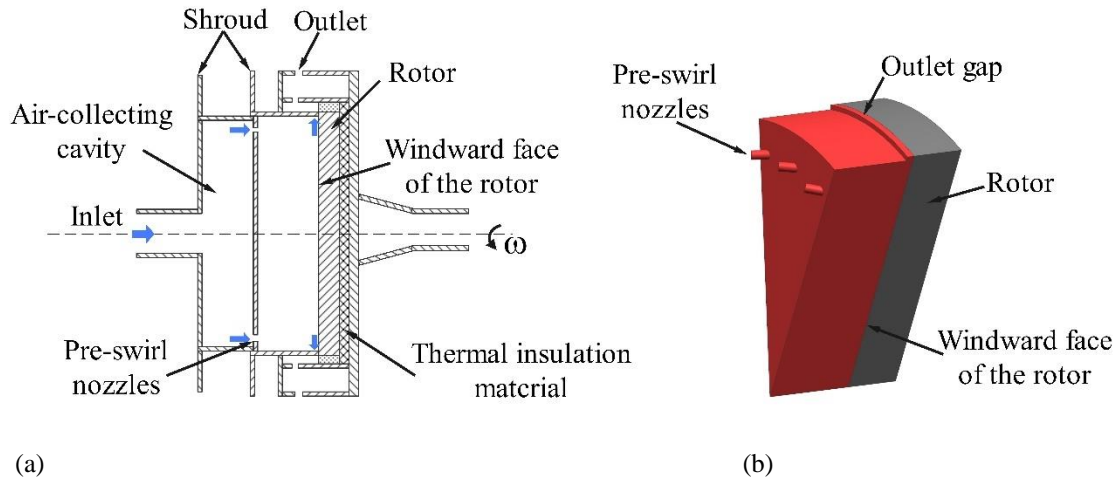


Fig. 2 (a) Experimental model and (b) simulation model for validation of turbulence models

The rotating disc is made of GH4169 superalloy, and its physical and thermodynamic parameters can be found in the literature (Guo et al., 2024).

2.2 Turbulence Model Validation

Numerous turbulence models have been employed in numerical computations up to this point. A Reynolds mean Navier–Stokes (RANS) simulation is the main method used in turbulence simulations (Cao et al., 2023). Numerous cavity flow computations in the past have utilized the high-Reynolds-number $k - \varepsilon$ turbulence model. In this paper, four turbulence models in CFX 17.2 are chosen for validation in order to determine which one can most accurately forecast the flow and heat transfer characteristics in the rotating cavity: *SST*, $k - \omega$, $k - \varepsilon$, and *RNGk - ε* . According to the characteristics of the TWD, we refer to the rotor–stator cavity and the co-rotating cavity to verify the accuracy of the turbulence models, respectively.

Xiang's (Xiang et al., 2007) experiment was used to validate the turbulence model of the rotor–stator cavity. In the experimental setup, coolant is introduced into the air collection cavity from the center and then directed into the disc cavity through a large-radius pre-swirl inlet. The disc features 30 pre-swirl holes with a pre-swirl angle of 30° . Following cooling of the rotating disc, coolant exits through an outlet located at the edge of the disc. A resistance wire is positioned at the edge of the disc to simulate heat exchange between the high-temperature gas and the rotating disc, while insulation material is placed on the rear side. The experimental operating conditions include a speed of 3000 rpm, a coolant flow rate of 200 kg/h, and heating power of 1100W. The experimental model and 1/12 simulation model are shown in Fig. 2.

As stated in the literature (Xiang et al., 2007), the following formula is true:

$$\Delta T = T_l - T_{in} \quad (1)$$

where ΔT is the excess temperature on the windward side, T_l is the local temperature, and T_{in} is the inlet temperature. Through the calculation of the excess temperature of the windward side, the influence of the inlet temperature is

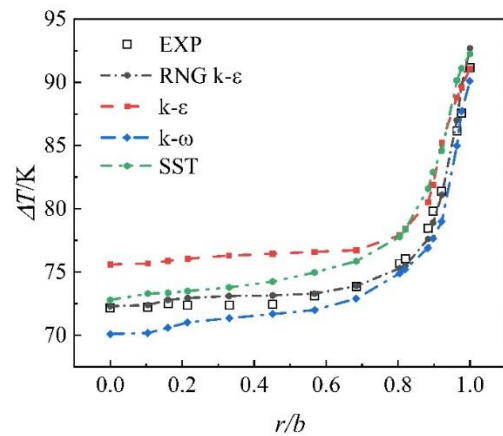


Fig. 3 Turbulence model validation results of the rotor–stator cavity

ignored. The excess temperature of the windward side predicted by numerical simulation is compared with the experimental data, as shown in the Fig. 3. The results show that the test data of the $k - \varepsilon$ turbulence model consistently demonstrate the same trend as the experimental data. Among them, the test data of *RNGk - ε* are in better agreement with the experimental data of high radius position. Therefore, in this paper, the *RNGk - ε* turbulence model is chosen for subsequent calculations.

Based on the experimental verification of the rotor–stator cavity, the simulation results of the *RNGk - ε* turbulence model in the co-rotating disc cavity are compared with the calculation results of literature (Owen & Pincombe, 1980), as follows:

$$\frac{u}{\bar{v}} = -\frac{\bar{v}}{U} \exp(-z/D) \sin(z/D) \quad (2)$$

$$U = Q/2\pi as \quad (3)$$

$$\bar{v} = -Q/2\pi rD \quad (4)$$

where u represents the local radial velocity, U represents the overall average radial velocity at the entrance, z/s represents the dimensionless axial distance, \bar{v} represents the tangential velocity of the non-viscous core region

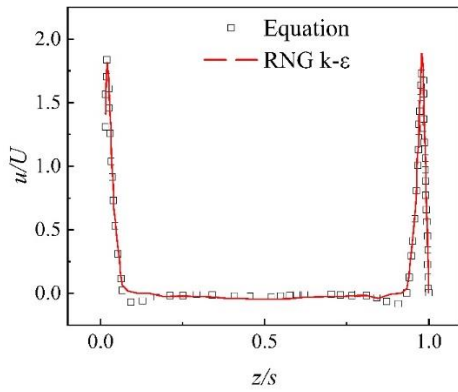


Fig. 4 Turbulence model validation results of the co-rotating disc cavity

(between Ekman layers on the rotating disc), D represents the one-third thickness of the Ekman layer, a represents the radial height of the entrance of the co-rotating cavity, s represents the axial width of the co-rotating cavity, and Q represents the inlet flow rate.

Figure 4 shows that the numerical calculation of $RNGk - \varepsilon$ turbulence model is in good agreement with the results in the literature. Therefore, the $RNG k - \varepsilon$ turbulence model is used in this paper to calculate the flow and heat transfer characteristics of the twin-web turbine disc cavity.

2.3 Boundary Conditions and Grids

The interface between the fluid and solid regions is used as a couple interface. A uniform heat flux boundary condition of 420000W/m^2 was applied to the top surface of the solid region near the high-temperature blade, and adiabatic boundary conditions were applied to the other walls of the fluid region. The coolant is an ideal gas. In Case₂, the three inlet flows are equal, and the total flow is the same as in Case₁. The total flow rate of both cases was 0.025kg/s , and the total inlet temperature was 700K . The outlet is an average static pressure outlet of 1MPa , and the rotor speed is 10000rev/min . Since this work mainly focuses on the convective heat transfer characteristics of the inner cavity, the boundary conditions of fluid domain 1 and fluid domain 2 do not change during the calculation.

Due to the boundary layer in the fluid domain near the solid domain, the temperature and velocity gradients are higher. Thus, the grids at the fluid–solid interface, coolant inlet and outlet, and receiver hole are encrypted. Liu et al. (2014) and Gao et al. (2017) suggested that the computational grid for the analysis of convective heat transfer in turbine blades should contain more than 15 units in the boundary layer. According to this, the boundary layer with 15 units near the walls of these three fluid domains was refined into a first-layer mesh of 0.05mm thickness. The growth rate was 1.1 and the $y+$ value computed by the $RNG k - \varepsilon$ turbulence model was less than 1. The model of Case₂ is taken as an example, and the grid diagram is shown in the Fig. 5.

Grid independence was verified using the maximum temperature (T_{max}) in the solid domain (TWD). Figure 6 presents the calculation of grid independence. When the number of meshes in Case₁ exceeded $4,985,955$ and the

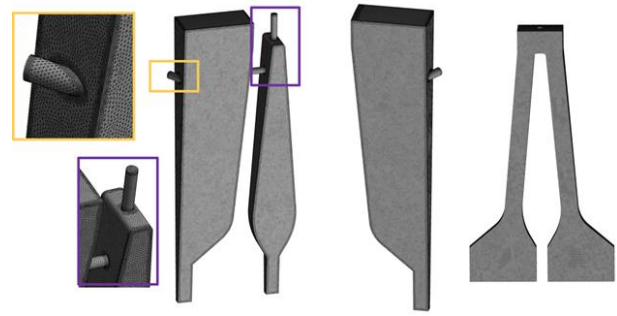


Fig. 5 Grid

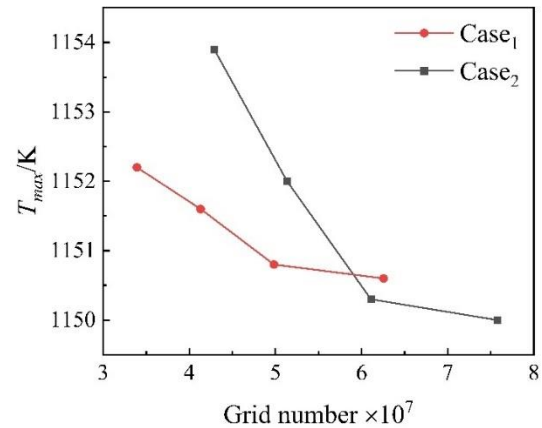


Fig. 6 Grid independence verification

number of meshes in Case₂ exceeded $6,108,524$, the variation in the T_{max} value was less than 0.2K . Considering the accuracy of the calculation and the reduction in computing resources, this grid number was selected for the subsequent calculation.

3. ANALYSIS AND DISCUSSION

3.1 Parameter Definition

(a) Swirl ratio Sr

The swirl ratio of the coolant in the rotating cavity is expressed as the ratio of the circumferential velocity of the airflow to the rotational speed of the rotating disc, and is defined as follows:

$$Sr = \frac{V_\varphi}{\omega r} \quad (5)$$

where V_φ is the circumferential speed of the coolant and ω is the rotation speed of the rotating disc.

(b) The rotation Reynolds number, Re_φ , is defined as follows:

$$Re_\varphi = \frac{\rho \omega b^2}{\mu} \quad (6)$$

(c) The dimensionless mass flow, C_m , is defined as follows:

$$C_m = \frac{m}{\mu b} \quad (7)$$

(d) The turbulence parameter, λ_T , is defined as follows:

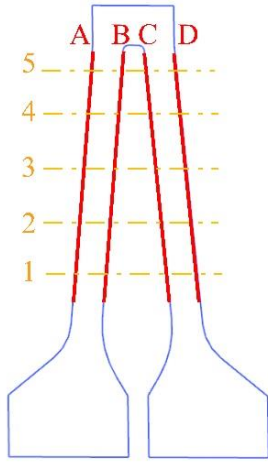


Fig. 7 Selection of feature points

$$\lambda_T = \frac{c_m}{Re_\phi^{0.8}} \quad (8)$$

where ρ is the density of ideal air, b is the outer radius of the turbine disc, which is defined as R_1 in this paper, m is the coolant flow into the entire cavity, and μ is the dynamic viscosity of the coolant.

(e) The radial temperature non-uniformity coefficient, T_{vr} , is defined in formula (9).

To express the turbine disc temperature gradient more intuitively, the characteristics of each set of five point temperatures were analyzed in four series to choose between the inner and outer walls of the ABCD, respectively, as seen in Fig. 7, before and after the temperature uniformity of the web.

The radial temperature nonuniformity coefficient of the turbine disc is represented by T_{vr} , which is defined as follows:

$$T_{vr} = \frac{S}{\bar{t}} \quad (9)$$

The smaller the value of T_{vr} , the better the radial uniformity.

$$S = \sqrt{\frac{1}{n} \sum_{i=1}^n (t_i - \bar{t})^2} \quad (10)$$

where \bar{t} is the average temperature of all feature points in the series, S is the temperature change, n is the number of feature points, and t_i is the temperature of that feature point.

(f) The normalized temperature, θ , is defined as follows:

$$\theta = \frac{t_n - t_{min}}{t_{max} - t_{min}} \quad (11)$$

where t_n , t_{max} , and t_{min} represent the temperature, maximum temperature, and minimum temperature of the turbine disc under different working conditions, respectively.

(g) The Nusselt number, Nu , is defined as follows:

$$Nu = \frac{qr}{\lambda(T_l - T_r)} \quad (12)$$

where q represents the heat flux, r represents the local radius, λ represents the thermal conductivity of the coolant, T_l represents the local temperature, and T_r represents the reference temperature; 700K was chosen as the reference temperature in this paper.

(h) The field synergy angle (FSA), β , is defined as follows:

$$\cos \beta = \frac{\vec{v} \cdot \text{grad} \vec{T}}{|\vec{v}| \cdot |\text{grad} \vec{T}|} \quad (13)$$

where \vec{v} represents the velocity gradient and $\text{grad} \vec{T}$ represents the temperature gradient.

Liu et al. (2014) points out that, in a rotating cavity, the cosine field $\cos \beta$, formed by the velocity field \vec{v} and the temperature gradient field $\text{grad} \vec{T}$, should be reduced as far as possible to increase the convective heat transfer coefficient; that is, the coordination angle between \vec{v} and $\text{grad} \vec{T}$ should be reduced.

3.2 Theoretical Analysis

In the rotor system, the cooling is mainly achieved via the influence of the relative total temperature, T_{rel}^* , of the coolant. This is calculated as follows:

$$T^* = T + \frac{V_z^2}{2c_p} + \frac{V_r^2}{2c_p} + \frac{V_\phi^2}{2c_p} \quad (12)$$

$$T_{rel}^* = T + \frac{V_z^2}{2c_p} + \frac{V_r^2}{2c_p} + \frac{(V_\phi - \omega r)^2}{2c_p} \quad (13)$$

where T is the static temperature, T^* is the absolute total temperature, T_{rel}^* is the relative total temperature in the rotating coordinate system, and V_z , V_r , and V_ϕ are the axial, radial, and circumferential velocity components, respectively.

The relationship between the absolute total temperature and the relative total temperature can be obtained by combining the above formulas, as follows:

$$T^* = T_{rel}^* + \frac{(\omega r)^2}{2c_p} (2Sr - 1) \quad (14)$$

In flow field analysis, the swirl ratio is a key factor, and only when its value is greater than 0.5 will it cause a temperature drop to the system.

Without regard to wall heat transfer, the following formula is true:

$$T_{rel,2}^* - T_{rel,1}^* = \frac{\omega^2 (r_2^2 - r_1^2)}{2c_p} \quad (15)$$

When the air flows out along the radial direction (i.e. $r_1 < r_2$), the temperature drop of the air flow increases with the increase in the radial flow and the turbine disc speed. This phenomenon indicates that the flow along the radius is important for the rotational cooling effect. Conversely, a flow against the radius results in an increase in relative total temperature and entropy production.

At the outlet of the receiver hole, the rotor–stator cavity 1 coolant is mixed with the inner cavity coolant. In the receiver holes, the swirl ratio of the coolant is one. After mixing with the coolant in the inner cavity, a large

local loss and an entropy increase are inevitably generated, and the swirl ratio will also cause a certain influence.

The circumferential momentum is considered to be conserved under ideal conditions without regard to the loss along the path and the local loss.

$$m_{rh}V_{\varphi,rh} + m_{ic}V_{\varphi,ic} = (m_{rh} + m_{ic})V_{\varphi,mix} \quad (16)$$

where m_{rh} and m_{ic} represent the mass flow of coolant through the receiver holes. In the inner cavity, $V_{\varphi,rh}$ and $V_{\varphi,ic}$ represent the circumferential velocity components of coolant at the receiver hole outlet and in the inner cavity, respectively, and $V_{\varphi,mix}$ represents the circumferential velocity components of the mixture in the inner cavity.

This can be obtained by combining the formula for the swirl ratio (5), as follows:

$$m_{rh}Sr_{rh} + m_{ic}Sr_{ic} = (m_{rh} + m_{ic})Sr_{mix} \quad (17)$$

where Sr_{rh} represents the swirl ratio of the coolant at the outlet of the receiver hole, Sr_{ic} represents the swirl ratio of the coolant in the inner cavity, and Sr_{mix} represents the swirl ratio of the mixed coolant.

In the two different inlet modes, $m_2 > m_1$ in Case₁ results in a higher degree of influence of Sr_{ic} on Sr_{mix} than that of the same mass flow in each rotating cavity in Case₂. Similarly, the total temperature of the mixture is more sensitive to the change in the total temperature in the inner cavity. In general, the swirl ratio in the inner cavity will be lower than is ideal due to losses caused by viscous resistance, etc. The swirl ratio of the coolant in the receiver hole is one, which significantly improves the flow state of the coolant in the inner cavity.

This can be obtained by combining formula (13) and formula (14), as follows:

$$m_{rh}c_pT_{rh}^* + m_{ic}c_pT_{ic}^* = (m_{rh} + m_{ic})c_pT_{mix}^* \quad (18)$$

where T_{rh}^* represents the total temperature of the coolant at the outlet of the receiver hole, T_{ic}^* represents the total

temperature of the coolant in the inner cavity, and T_{mix}^* represents the total temperature of the mixed coolant.

The total temperature of the coolant at the nozzle outlet in Case₂ is relatively low. Also, the total temperature of the coolant in Case₁ is inevitably higher than that in Case₂, due to the viscous resistance during radial outflow. In both cases, as a result of the high local loss at the receiver hole and heat transfer at the top of the rotor, the total temperature of the coolant passing through the receiver hole is inevitably higher than that of the coolant in the inner cavity, and the relative total temperature rise of the air flow after mixing is also higher. This is disadvantageous to the cooling of the large-radius rotor. In contrast, the cooling efficacy of the large-radius pre-swirl inlet approach is conspicuously superior to that of the central inlet mode. It can effectively lower the total temperature of the coolant at the receiver hole and mitigate the impact of the increasing temperature of the mixture within the inner cavity, thereby enhancing the cooling efficiency.

4. RESULTS AND DISCUSSION

4.1 Flow and Heat Transfer Characteristics

As shown in Fig. 8, in Case₁, the impact wall of the coolant in the axial channel at the bottom of the rotating cavity forms a more sufficient disturbance vortex, and the angle of the coolant in the axial channel with the direction of temperature field changes over time. Therefore, the jet impinges on the back wall of the rotating cavity, forming a region where the β between the axial channel and the entrance of the three rotating cavities is small. After entering the rotating cavities, the coolant is purged to a high radius position under the action of centrifugal force and Coriolis force. Interestingly, the coolant creates a disturbance at the static wall in the two rotating disc cavities, resulting in a low FSA region in a smaller area. In Case₂, this is different. Due to the high pre-swirl of the

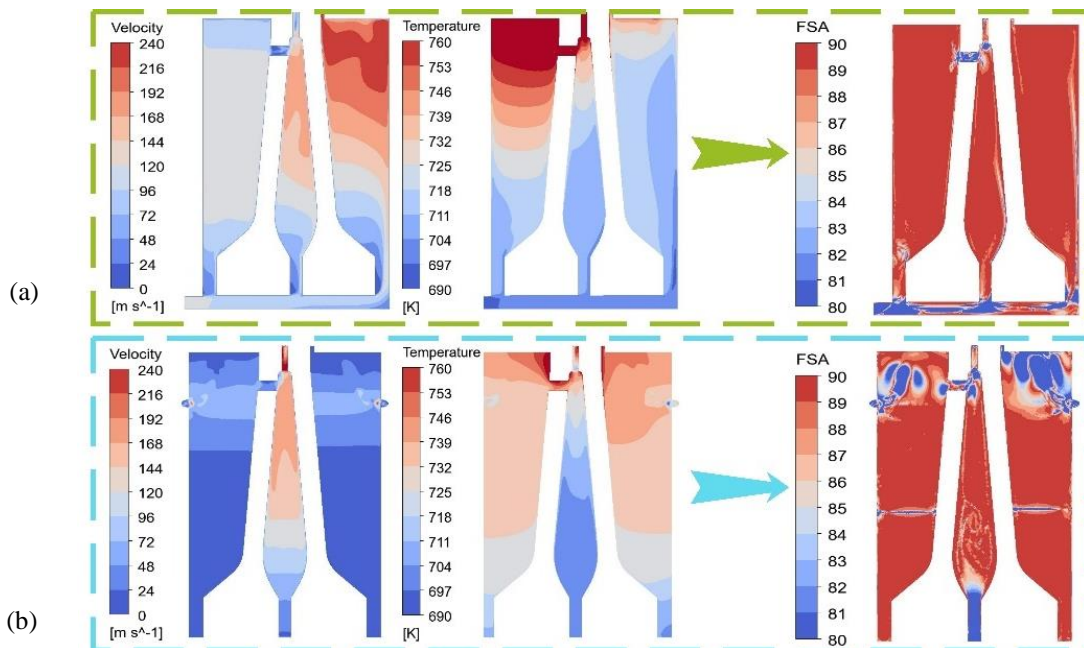


Fig. 8 FSA distribution of (a) Case₁ and (b) Case₂

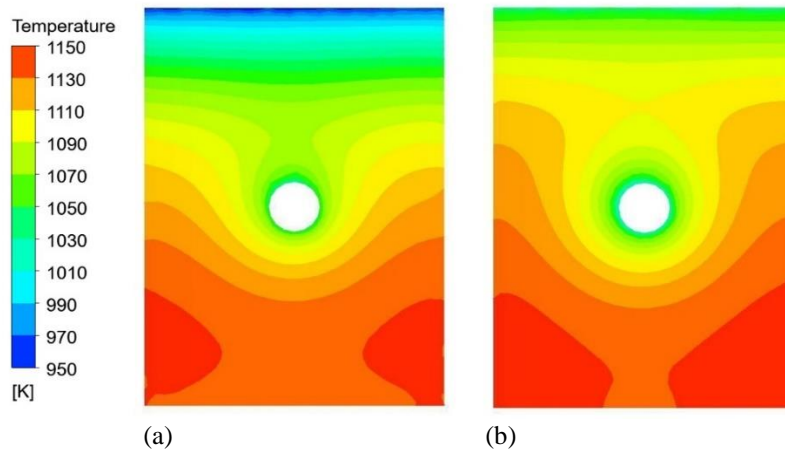


Fig. 9 Temperature distribution on the disc edge of (a) Case₁ and (b) Case₂

two rotor–stator cavities, the coolant flows through the pre-swirl nozzles on both sides to form jets impacting the outer wall of the turbine disc, and deflects upward to form two disturbance vortices, resulting in a large region with a small FSA value at a large radius. In addition, at the narrow entrance of the inner cavity, the air flow is restricted and there are strong turbulence and boundary layer effects. Turbulence destroys the rotational structure of the air flow, making the air flow unable to fully expand and rotate. This also results in smaller FSA values. It is worth noting that both cases produce small FSA values at the entrance, channel, and outlet of the receiver holes. In Case₂, due to the influence of the large-radius inlet pre-swirl mode, the region formed is larger and more evident. Since the turbine disc has a large temperature gradient at the high radius position, the low FSA region generated at the high radius position is conducive to improving the cooling effect of the turbine disc.

Figure 9 displays the temperature distribution on the disc edge. On the disc's edge, the temperature distribution is essentially symmetrical. The maximum temperature can be found at the edge of the disc near the front web. The maximum temperature of the disc edge is not significantly different under the computed working conditions. In Case₁, the disc edge with the sealed slit outlet cooled more effectively, whereas, in Case₂, the temperature was lower close to the outlet-mid in the disc edge's center. This is because, as the coolant enters the turbine cavity from the axial inlet at the bottom of the turbine disc, it flows more freely into the rotor–stator cavity 2 in Case₁, which results in a superior cooling performance. Furthermore, the greater axial temperature gradient of the disc edge is brought about by the increased coolant flow rate in rotor–stator cavity 2 in Case₁, particularly within the gas supply hole to the back web disc edge.

The convective heat transfer coefficients near the front and rear web inner and outer walls are illustrated in Fig. 10. It is evident from Fig. 10 (a) and (b) that, in the two rotor–stator cavities, Case₁ exhibits a significantly higher convective heat transfer coefficient than Case₂. This can be attributed to the fact that, in Case₁, the coolant flows in from the inlet-mid, resulting in a radial flow that induces stronger shear and disturbance at the wall surface, thereby enhancing the convective heat transfer coefficient.

This effect is particularly pronounced in rotor–stator cavity 2, where the mass flow and the velocity of coolant are higher. However, both cases exhibit a trend of an initially increasing convective heat transfer coefficient and then a decreasing convective heat transfer coefficient within rotor–stator cavity 1, due to the convergence of the coolant at the receiver hole, leading to a small oscillation.

On the contrary, in the inner cavity, due to the low and uneven flow in the inner cavity of Case₁, the convective heat transfer coefficient is lower than that in Case₂. The presence of a standing vortex under the receiver hole also contributes to significant oscillations in convective heat transfer coefficient. The decrease in convective heat transfer coefficient at high radius positions hinders improvements in cooling efficiency.

The Nusselt numbers of the outer wall of the front web, inner wall of the front web, inner wall of the back web, and outer wall of the back web are shown in Fig. 11. Likewise, owing to a more pronounced temperature gradient at the disc edge, there is a discernible radial increase in Nusselt numbers across all four walls. A notable difference is that, within rotor–stator cavity 1, the high pre-swirl ratio in Case₂ generates a jet, impacting its wall surface; meanwhile, the converging coolant from below creates a localized peak in Nusselt numbers.

In Case₁, coolants exhibit axial velocity upon entering an internal cavity, where they initially impact its back web inner wall surface, causing deflection. This is also shown in Fig. 10(d) that the convective heat transfer coefficient of Case₁ is higher at the low radius position. Furthermore, along the radial flow direction, the axial velocity of the coolant gradually decreases, and the coolant is separated from the inner wall of the back web, resulting in a unique trend; the Nusselt number on the back web first decreases and then increases, while the Nusselt number on the inner wall of the front web increases. Conversely, for Case₂, coolants flow radially within an internal cavity, yielding relatively uniform Nusselt distributions across both surfaces therein. Similarly, both cases experience localized drops downstream of their respective outlet holes, attributed to angular viscous dissipation stemming from turbulent backflows.

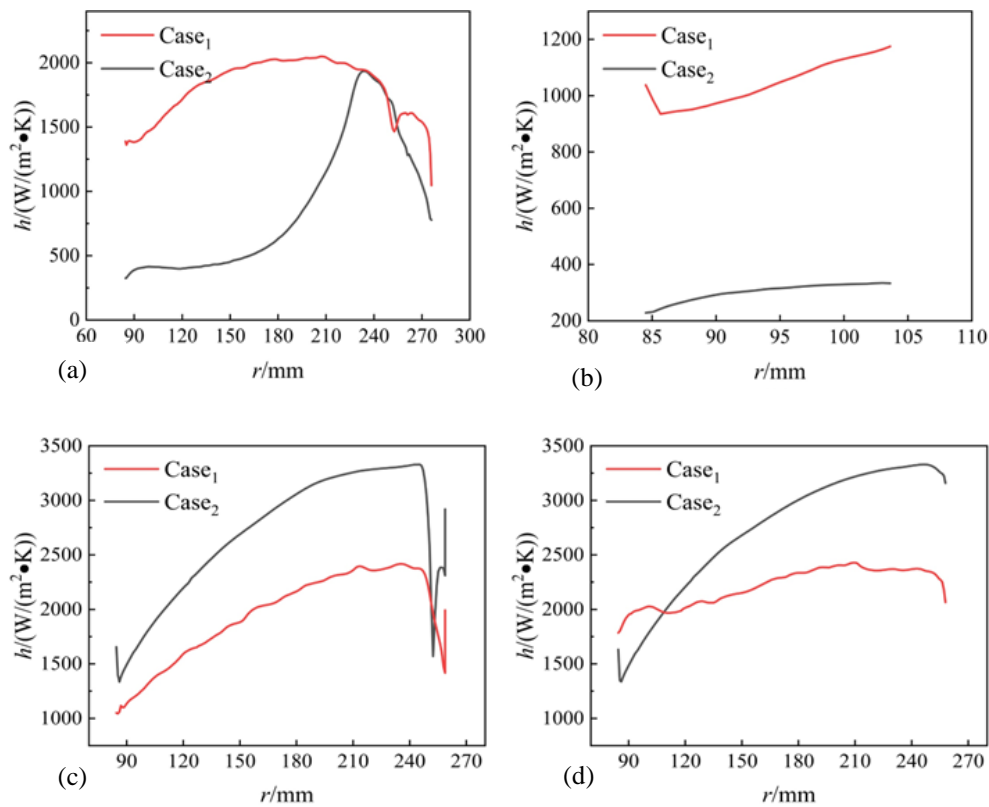


Fig. 10 Convective heat transfer coefficients near the (a) front web outer wall, (b) bank web outer wall, (c) front web inner wall, and (d) back web inner wall

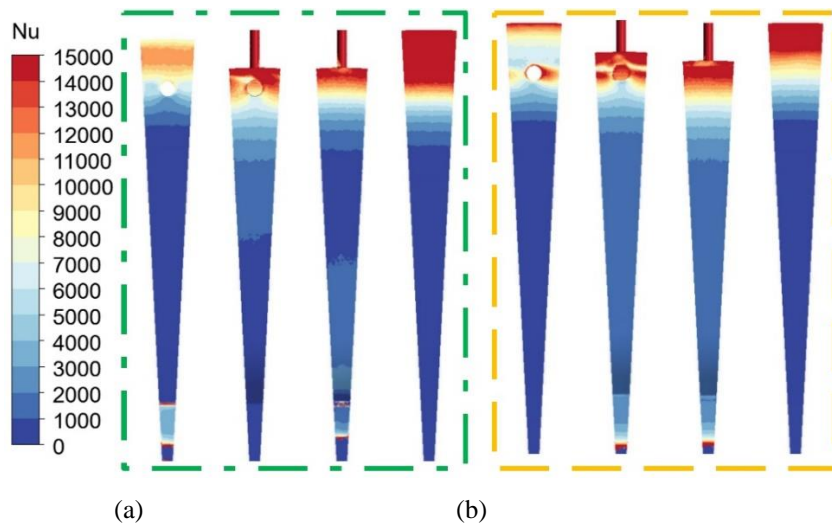


Fig. 11 Nusselt number of (a) Case 1 and (b) Case 2

4.2 Effect of Operating Conditions

The turbulence parameter, λ_T , which is crucial for regulating the temperature and flow heat transfer in the disc surface, has been extensively employed in rotating cavity research (Bai et al., 2022). It is also the control parameter for the fluid flow line structure in the disc cavity.

We examined the independent impacts of dimensionless mass flow and rotational Reynolds number on turbine disc temperature. Furthermore, under the same turbulence settings, the sensitivity of the heat transfer characteristics to these two parameters' impacts was also studied.

4.2.1 Effect of the dimensionless mass flow

The rotating cavities' coolant flow condition in Case 1, as depicted in Fig. 12, varies as the dimensionless mass flow rate increases. Due to the entrainment effect, the majority of the airflow will swiftly reach the rotor surface boundary layer as it enters the rotor–stator cavity. Afterwards, the air flow expands radially outward, forming a high-radius core region where a ring vortex is present. The air flow in the annular vortex in the core region is mostly circumferential and has a radial velocity of about zero. The temperature distribution in rotor–stator cavity 1 increases as a result of increased coolant distribution into the inner cavity and rotor–stator cavity 2,

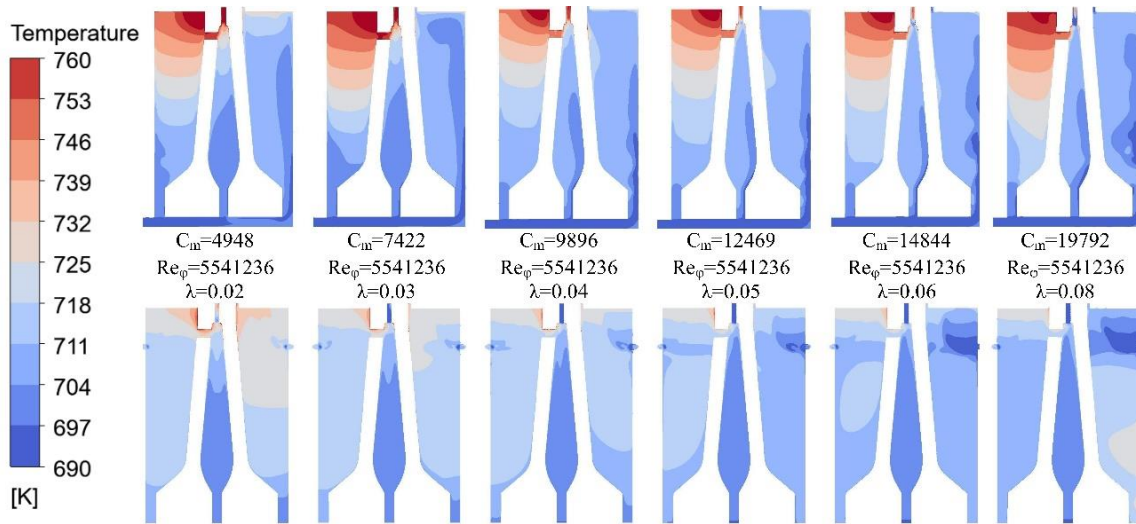


Fig. 12 Temperature distribution under different dimensionless mass flow rates

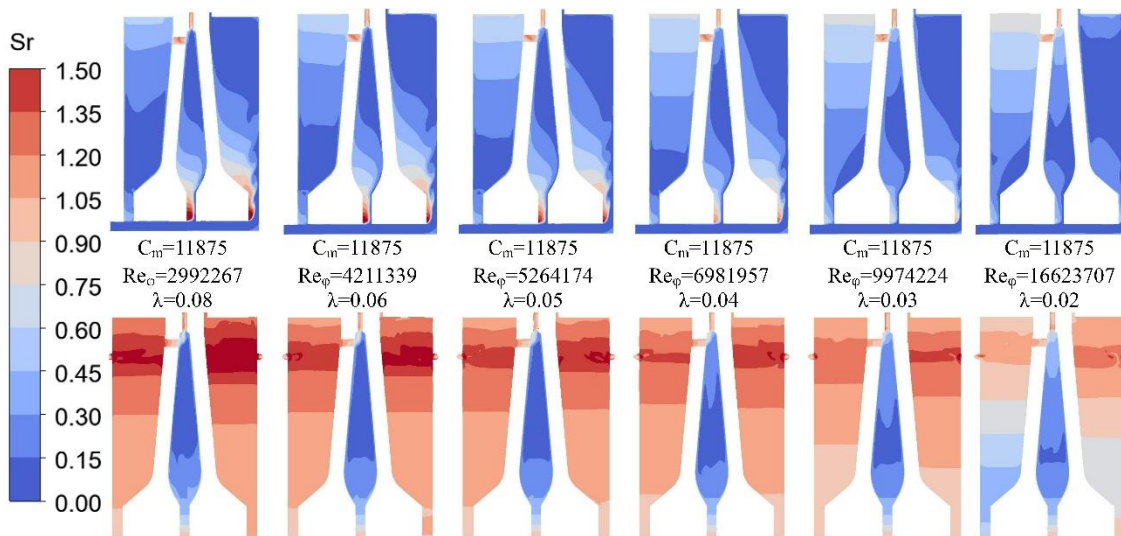


Fig. 13 Temperature distribution under different rotational Reynolds numbers

but there is a notable decrease in the angular vortex at the high-radius position and a significant reduction in the high-temperature region. Additionally, in rotor–stator cavity 2, the influence of jet momentum on the coolant flow characteristics within the cavity keeps growing. This results in increased turbulence at the cavity’s inlet and the boundary layer, which generates more eddy currents outside the stator surface’s boundary layer. This increases energy loss but also greatly enhances cooling efficiency.

In Case₂, the uniform flow rate makes the local high temperature region in the partial rotating cavity significantly decrease. The pre-swirling jet’s impact on the flow condition in the rotor–stator cavity increases dramatically as the inlet flow rate rises. A pair of neighbouring but opposing vortices form at the large-radius jet outlet in rotor–stator cavity 1 as a result of the receiver hole’s action, and one of them enters the inner cavity through the receiver hole. Secondary flow is also produced by the jet’s impact on the turbine disc’s outer wall, which is often the area most impacted by the pre-swirling jet’s impact. Similar to this, a disturbance vortex also forms at the high-radius site of the jet’s impact in rotor–stator cavity 2, as a result of the radial outflow. The

effect of the jet’s impact is much enhanced and the temperature distribution within the cavity is greatly improved with an increase in the inlet flow rate. This is particularly evident at high-radius positions, particularly those with higher nozzle exits.

4.2.2 Effect of the Rotational Reynolds Number

The distribution of swirl ratio in the disc cavity with the variation in rotational Reynolds number is shown in Fig. 13. In Case₁, the axial jet strikes the back wall, creating a region near the entry with a comparatively high local swirl. The rotor entrainment effect steadily increases, and the local high swirl ratio region gradually decreases as the rotational Reynolds number increases. As the flow area approaches the rotor surface in rotor–stator cavity 2, the swirl ratio rises. The result of flow entrainment at various points within the rotor–stator cavity and along the formed turbulent boundary layer on the revolving disc have distinct flow characteristics. It is important to note that the receiver hole’s action causes the swirl ratio in rotor–stator cavity 1 to increase as the radial height increases. In Case₂, the swirl ratio of the two rotor–stator cavities gradually reduce as the rotational Reynolds

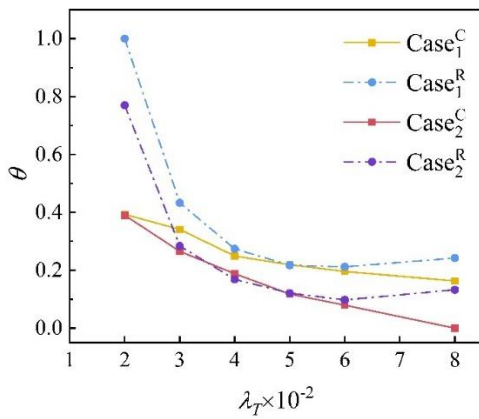


Fig. 14 Normalized temperature changes with turbulence parameter

number increases. However, the inner cavity’s swirl ratio progressively rises as a result of the receiver hole’s constraint. Additionally, the swirl ratio in the core region will fall first because of the impact of the Ekman layer close to the rotating disc. The inner cavity’s swirl ratio exhibits a lower, middle, and higher two-side trend.

Interestingly, as λ_T becomes larger, the jet’s effect becomes more significant, while the effect of rotor entrainment is slightly weakened. As the turbulence parameter of Case₁ increases, the tangential velocity component associated with cooling air near the rotor surface is usually higher than the local rotor speed. In this case, the cooling air is sufficient to maintain the Ekman layer associated with the rotor, the rotor contains only a small amount of circulating air, and the flow characteristics are dominated by jet momentum, which is particularly evident in the inner cavity and rotor–stator cavity 2. However, the coolant in rotor–stator cavity 1 exhibits different flow characteristics due to the uneven structure of the cavity and the subsequent flow distribution. In Case₂, the increasing influence of jet momentum on flow characteristics is more evident. In addition, the relative influence of rotor entrainment is reduced, so that the local surface heat flux characteristics are determined mainly by the trajectory and distribution of the fluid originating in the pre-swirling jet.

4.2.3 Effect of the Turbulence Parameter

Figure 14 displays the normalized temperature.

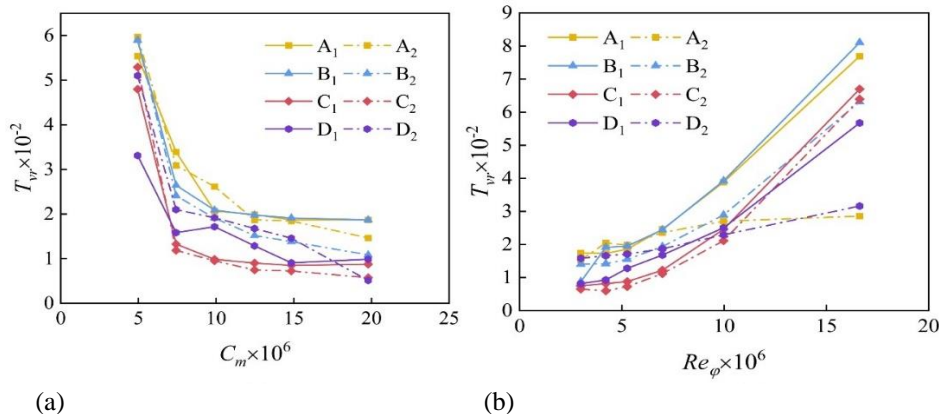


Fig. 15 Radial temperature non-uniformity coefficient changes with changes in (a) dimensionless mass flow and (b) rotational Reynolds number

$Case_1^C$ and $Case_1^R$ represent the change curves of Case₁ with dimensionless mass flow and rotational Reynolds number, respectively, and $Case_2^C$ and $Case_2^R$ are the same. Both situations have a similar change trend. While the maximum temperature gradually drops with an increasing dimensionless mass flow, this decreasing trend also gradually reduces. It is worth noting that the cooling effect of Case₂ is much stronger than that of Case₁. In combination with Fig. 12 and Fig. 13, this is due to the inlet vortex generated by the axial inlet in rotor–stator cavity 1, which hinders the inflow of the coolant. More coolant flows into the inner cavity and rotor–stator cavity 2, resulting in a relatively poor cooling effect on the front web wall, thus limiting further cooling temperature reduction. Both cases tend to show a decrease first and then an increase with an increase in the rotational Reynolds number, which is because most of the swirl ratio distribution of the coolant in the cavity gradually decreases with the increase in the rotor speed. When the swirl ratio is close to one, the relative movement between the coolant and the rotor is small, and the friction loss is low. In general, the twin-web turbine disc cavity systems with a large-radius inlet pre-swirl mode have better cooling effects.

Fascinatingly, the normalized temperature changes tend to flatten off gradually as turbulence parameters grow. Furthermore, a change in the rotational Reynolds number can significantly affect the turbine disc temperature when the turbulence parameters are minimal. A big oscillation in temperature will result from a minor oscillation in rotational Reynolds number under the same turbulence settings. The jet impact becomes more pronounced as turbulence parameters rise, and dimensionless mass flow plays a bigger and bigger part in regulating flow and heat transfer, as well as progressively taking the lead in determining turbine disc temperature. The temperature changes clearly show this.

The variation in the radial temperature non-uniformity coefficient with the dimensionless mass flow and rotational Reynolds number is shown in Fig.15. The subscript 1 is the feature point of Case₁, and the subscript 2 is the feature point of Case₂. Generally speaking, the variation in the radial temperature uniformity of the inner and outer walls of the TWD is the same in the two inlet modes. In particular, Fig. 15 (a) shows a rapid decline

followed by a gradual levelling off. Notably, Case₂ exhibits better radial temperature uniformity following the increase in dimensionless mass flow rate and rotational Reynolds number. In particular, in Fig. 15 (b), compared with feature points A₁ and D₁, points A₂ and D₂ decrease by 63% and 44%, respectively. This indicates that the large-radius inlet pre-swirl mode results in lower local thermal stress. In the inner cavity, a jet is formed at the outlet of the receiver holes, which will result in a better cooling effect on the back wall of the inner cavity. However, standing vortices are formed at the large-radius outlet of the receiver hole, which is also the reason for the relatively extreme temperature non-uniformity coefficients at points B and C in the two different inlet modes.

4. CONCLUSION

In this paper, a twin-web turbine disc with a single side receiver hole is established. Through theoretical analysis and numerical simulation, the effects of two different coolant inlet modes, a high radius inlet pre-swirl mode and a central inlet mode on the flow and heat transfer characteristics of the disc cavity were studied. The main conclusions and findings of the study are as follows.

1. The two different inlet modes have different influences on the cooling performance of the turbine disc. The central inlet mode results in an uneven coolant flow distribution in each rotating cavity, resulting in a higher convective heat transfer coefficient and a higher Nusselt number in the two rotor–stator cavities. However, the large-radius inlet pre-swirl mode generates disturbance vortices in the high-radius area, which improves the cooling effect in the high-temperature area and can effectively improve the flow state and heat transfer in the inner cavity.

2. The coolant flow characteristics in the rotating cavity change significantly with the change in operating conditions. With an increase in the dimensionless mass flow rate, the jet effect becomes significant, which improves the cooling efficiency but also increases energy loss. In Case₁, the impact of uneven flow is more severe, while, in Case₂, the enhancement of pre-swirling jet significantly reduces the local high-temperature region. With an increase in the rotational Reynolds number, the entrainment effect of the rotor is enhanced, gradually replacing the jet momentum as the dominant factor of the flow state in the disc cavity, leading to the swirl ratio in the disc cavity being gradually reduced.

3. The variation in dimensionless temperature and radial temperature uniformity with the change in operating conditions is similar in the two inlet modes. With an increase in turbulence parameters, the jet effect replaces the rotor entrainment effect as the main driving force for regulating heat transfer, which makes the normalized temperature change and the radial temperature non-uniformity coefficient smooth. In contrast, Case₂ has better cooling performance.

It is worth noting that this paper mainly focuses on the inlet modes of the coolant, and only gives a limited description of the twin-web turbine disc cavity. In future

works, a more comprehensive analysis should be carried out, taking into account real operating conditions. However, this study generates valuable insights that provide a research basis for the optimal design of the disc cavity of a twin-web turbine.

ACKNOWLEDGEMENTS

This research was funded by the National Science and Technology Major Projects of China, grant number Y2022-III-0003-0012.

CONFLICT OF INTEREST

The authors declare no conflicts of interest.

AUTHORS CONTRIBUTION

Y. T. Guo: Conceptualization, investigation, methodology, software, validation, writing—original draft; **S. F. Wang:** Conceptualization, funding acquisition, project administration, supervision, writing—review and editing; **W. J. Shen:** software, validation, writing—review and editing. All authors have read and agreed to the published version of the manuscript.

REFERENCES

- Bai, Y., Luo, X., & He, J. (2022). Influence of turbulence parameters on flow characteristics of cavity with tubed vortex reducer. *Journal of Aerospace Power*, 37(6), 1295-1305
- Bricaud, C., Geis, T., Dullenkopf, K., & Bauer, H. J. (2007). Measurement and Analysis of Aerodynamic and Thermodynamic Losses in Pre-Swirl System Arrangements. *Proceedings of the ASME Turbo Expo 2007: Power for Land, Sea, and Air*. 2007. <https://doi.org/10.1115/gt2007-27191>
- Cao, Y., Xu, R., & Jiang, P. (2023). Physics-informed machine learning based RANS turbulence modeling convection heat transfer of supercritical pressure fluid. *International Journal of Heat and Mass Transfer*, 201, 123622. <https://doi.org/10.1016/j.ijheatmasstransfer.2022.123622>
- Gao, W. J., Yue, Z. F., Li, L., Zhao, Z. N., & Tong, F. J. (2017). Numerical simulation on film cooling with compound angle of blade leading edge model for gas turbine. *International Journal of Heat and Mass Transfer*, 115, 839–855. <https://doi.org/10.1016/j.ijheatmasstransfer.2017.07.105>
- Gong, W., Liu, G., Wang, J., Wang, F., Lin, A., & Wang, Z. (2022). Aerodynamic and thermodynamic analysis of an aero-engine pre-swirl system based on structure design and performance improvement. *Aerospace Science and Technology*, 123, 107466. <https://doi.org/10.1016/j.ast.2022.107466>
- Guo, Y., Wang, S., & Shen, W. (2024). Genetic optimization of twin-web turbine disc cavities in

- aeroengines. *Energies*, 17(17), 4346. <https://doi.org/10.3390/en17174346>
- Jarzombek, K., Dohmen, H. J., Benra, F. K., & Schneider, O. (2006). Flow Analysis in Gas Turbine Pre-Swirl Cooling Air Systems: Variation of Geometric Parameters. *Proceedings of the ASME Turbo Expo 2006: Power for Land, Sea, and Air*. <https://doi.org/10.1115/gt2006-90445>
- Kim, Y. I., & Song, S. J. (2019). Unsteady measurement of core penetration flow caused by rotating geometric non-axisymmetry in a turbine rotor-stator disc cavity. *Experimental Thermal and Fluid Science*, 107, 118–129. <https://doi.org/10.1016/j.expthermflusci.2019.05.017>
- Kong, X., Huang, T., Liu, Y., Chen, H., & Lu, H. (2022). Effects of pre-swirl radius on cooling performance of a rotor-stator pre-swirl system in gas turbine engines. *Case Studies in Thermal Engineering*, 37, 102250. <https://doi.org/10.1016/j.csite.2022.102250>
- Lewis, P., Wilson, M., Lock, G. D., & Owen, J. M. (2008). Effect of radial location of nozzles on performance of preswirl systems: A computational and theoretical study. *Proceedings of the Institution of Mechanical Engineers Part a Journal of Power and Energy*, 223(2), 179–190. <https://doi.org/10.1243/09576509jpe689>
- Li, L., Tang, Z., Li, H., Gao, W., Yue, Z., & Xie, G. (2020). Convective heat transfer characteristics of twin-web turbine disk with pin fins in the inner cavity. *International Journal of Thermal Sciences*, 152, 106303. <https://doi.org/10.1016/j.ijthermalsci.2020.106303>
- Li, L., Tang, Z., Li, H., Tong, F., & Gao, W. (2019). Multidisciplinary design optimization of twin-web turbine disk with pin fins in inner cavity. *Applied Thermal Engineering*, 161, 114104. <https://doi.org/10.1016/j.applthermaleng.2019.114104>
- Liao, G., Wang, X., & Li, J. (2014). Numerical investigation of the pre-swirl rotor-stator system of the first stage in gas turbine. *Applied Thermal Engineering*, 73(1), 940–952. <https://doi.org/10.1016/j.applthermaleng.2014.08.054>
- Lin, A., Liu, G., Li, P., Zhang, Z., & Feng, Q. (2022). Theoretical and experimental evaluations of pre-swirl rotor-stator system with inner seal bypass configuration for turbine performance improvement. *Energy*, 258, 124760. <https://doi.org/10.1016/j.energy.2022.124760>
- Lin, A., Liu, G., Wang, X., & Feng, Q. (2021). Comprehensive evaluations on performance and energy consumption of pre-swirl rotor-stator system in gas turbine engines. *Energy Conversion and Management*, 244, 114440. <https://doi.org/10.1016/j.enconman.2021.114440>
- Liu, G., Gong, W., Wu, H., Pang, L., & Lin, A. (2021a). Theoretical and experimental evaluation of temperature drop and power consumption in a cover-plate pre-swirl system for gas turbine cooling. *Case Studies in Thermal Engineering*, 27, 101221. <https://doi.org/10.1016/j.csite.2021.101221>
- Liu, Y., Lu, B., Kong, X., & Chen, H. (2023). Experimental study on the outlet flow field and cooling performance of vane-shaped pre-swirl nozzles in gas turbine engines. *Case Studies in Thermal Engineering*, 44, 102878. <https://doi.org/10.1016/j.csite.2023.102878>
- Liu, Y., Yue, B., Kong, X., Chen, H., & Lu, H. (2021b). Design and performance analysis of a vane shaped rotating receiver hole in high radius pre-swirl systems for gas turbine cooling. *Aerospace Science and Technology*, 115, 106807. <https://doi.org/10.1016/j.ast.2021.106807>
- Liu, Z., Ye, L., Wang, C., & Feng, Z. (2014). Numerical simulation on impingement and film composite cooling of blade leading edge model for gas turbine. *Applied Thermal Engineering*, 73(2), 1432–1443. <https://doi.org/10.1016/j.applthermaleng.2014.05.060>
- Ma, A., Liu, F., Zhou, T., & Hu, R. (2021). Numerical investigation on heat transfer characteristics of twin-web turbine disk-cavity system. *Applied Thermal Engineering*, 184, 116268. <https://doi.org/10.1016/j.applthermaleng.2020.116268>
- Ma, A., Wu, Q., Zhou, T., & Hu, R. (2022). Effect of inlet flow ratio on heat transfer characteristics of a novel twin-web turbine disk with receiving holes. *Case Studies in Thermal Engineering*, 34, 101990. <https://doi.org/10.1016/j.csite.2022.101990>
- Ma, J., Liu, G., Li, J., Wu, C., Zhang, Y., & Lin, A. (2024). Evaluation of low power consumption and temperature drop potential in an aero-engine pre-swirl system for turbine performance improvement. *Applied Energy*, 359, 122601. <https://doi.org/10.1016/j.apenergy.2023.122601>
- Owen, J. M., & Pincombe, J. R. (1980). Velocity measurements inside a rotating cylindrical cavity with a radial outflow of fluid. *Journal of Fluid Mechanics*, 99(1), 111–127. <https://doi.org/10.1017/s0022112080000547>
- Xia, Z., Wang, S., & Zhang, J. (2020). A Novel design of cooling air supply system with dual row pre-swirl nozzles. *Journal of Applied Fluid Mechanics*, 13(04). <https://doi.org/10.36884/jafm.13.04.30957>
- Xiang, L., Guoqiang, X., Zhi, T., & Shuiting, D. (2007). Flow and heat transfer in rotor-stator system with pre-swirl angle of 30°. *Beijing Hangkong Hangtian Daxue Xuebao*, 33(03), 290. <https://bhxb.buaa.edu.cn/EN/abstract/abstract9550.shtml>
- Yan, C., Yin, Z., Shen, X., Mi, D., Guo, F., & Long, D. (2020). Surrogate-based optimization with improved support vector regression for non-circular vent hole on aero-engine turbine disk. *Aerospace Science and*

Technology, 96, 105332.
<https://doi.org/10.1016/j.ast.2019.105332>

Zhang, F., Wang, X., & Li, J. (2016a). Numerical investigation of flow and heat transfer characteristics in radial pre-swirl system with different pre-swirl nozzle angles. *International Journal of Heat and Mass Transfer*, 95, 984–995.
<https://doi.org/10.1016/j.ijheatmasstransfer.2016.01.010>

Zhang, M., Gou, W., Li, L., Yang, F., & Yue, Z. (2016b). Multidisciplinary design and multi-objective optimization on guide fins of twin-web disk using Kriging surrogate model. *Structural and Multidisciplinary Optimization*, 55(1), 361–373.
<https://doi.org/10.1007/s00158-016-1488-0>

Zhang, M., Gou, W., Yao, Q., Li, L., & Yue, Z. (2017).

Investigation on heat transfer characteristic and optimization of the cooling air inlet for the twin-web turbine disk. *Journal of Physics Conference Series*, 885, 012011. <https://doi.org/10.1088/1742-6596/885/1/012011>

Zhang, M., Yao, Q., Sun, S., Li, L., & Hou, X. (2020). An efficient strategy for reliability-based multidisciplinary design optimization of twin-web disk with non-probabilistic model. *Applied Mathematical Modelling*, 82, 546–572.
<https://doi.org/10.1016/j.apm.2020.01.066>

Zhou, K., & Zhou, C. (2020). Effects of upstream Rankine vortex on tip leakage vortex breakdown in a subsonic turbine. *Aerospace Science and Technology*, 99, 105776. <https://doi.org/10.1016/j.ast.2020.105776>